




Lane formation of colloidal particles driven in parallel by gravityMarc Isele ¹, Kay Hofmann ^{1,*}, Artur Erbe ², Paul Leiderer¹ and Peter Nielaba^{1,†}¹*Physics Department, University of Konstanz, 78457 Konstanz, Germany*²*Helmholtz-Zentrum Dresden-Rossendorf, 01328 Dresden, Germany*

(Received 1 June 2023; accepted 28 August 2023; published 22 September 2023)

We investigate the lane formation in nonequilibrium systems of colloidal particles moving in parallel that are driven by the force of gravity. For this setup, an experimental implementation of a channel on a slope can be conceptualized. We employ the Brownian dynamics algorithm and confine the repulsive particles with hard walls based on the solution of the Smoluchowski equation in the half space. A difference of the driving force acting on the colloids could be achieved by using two spherical particle types with differing diameters but equal mass density. First, we investigate how a difference in the channel slope affects the lane formation of the systems, after which we analyze the lanes that formed. We find that the large particles push the small particles to the walls, resulting in exclusively small particle lanes at the walls. This contrasts the equilibrium state, where depletion forces push the larger particles to the walls. Additionally, we have a closer look at the mechanisms by which the lanes form. Finally, we find system parameter values that foster lane formation to lay the foundation for an experimental realization of our proposed setup. To round this off, we give an exemplary calculation of the slope angle needed to get the experimental system into a state of lane order. With the examination of lane order in systems that are driven in parallel, we hope to deepen our understanding of nonequilibrium order phenomena.

DOI: [10.1103/PhysRevE.108.034607](https://doi.org/10.1103/PhysRevE.108.034607)**I. INTRODUCTION**

In systems of individuals that move with different speeds, spontaneous order formation can occur. One of these nonequilibrium order phenomena is called lane formation, where the individuals align into parallel streams of different velocities. Systems in which lane order can be observed include pedestrians [1–3], ants [4], molecular motors [5,6], and bacteria [7]. In this ordered state, the transport efficiency of the individual rises significantly [4–6]. In confined systems, a lane order can even be mandatory to exhibit any transport at all [1,2].

Nonequilibrium order phenomena are to this day not understood well enough [8]. A commonly used tool to gain more insight into these phenomena are colloidal systems. Such phenomena include collective behavior [9–12] and band formation [13], as well as the previously mentioned lane formation [14,15]. The formation of lanes was found in counterdriven systems with electric fields [16–18], gas models, dipolar systems [19], ionic mixtures, plasmas [20,21], and systems of attractive particles [22]. The influence of hydrodynamic interactions on the stability of lanes was investigated as well [23,24].

While most simulations and experiments with colloidal particles have been performed on counterdriven particles, to our knowledge, so far it has not been shown whether colloids moving in parallel can exhibit lane formation, as well. To achieve a separation into lanes, it is mandatory to have a difference of particle transport [13,15]. We obtain this difference

by using the force of gravity as the driving force and two particle types with differing diameters. With the assumption of equal mass density of the particles, the driving force is then proportional to the mass of the respective particle.

In this work we investigate the emergence of lanes and features thereof in these systems. We found that the lanes, which form with an increase in driving force, always consist of small particles at the walls. During the formation of lanes, the large particles push their small counterparts to the wall, hence our naming this the “funneling effect.” In contrast to this, in systems where no driving force is applied, mostly large particles inhabit the space close to the walls because of entropic depletion forces [25]. This marks a significant qualitative difference between equilibrium and nonequilibrium states. We also have a closer look at the lane formation mechanism, as well as a set of system parameters that facilitate lane formation. Finally, we calculate the slope angle needed to reach critical lane formation in an exemplary experimental system.

This work is structured as follows: first, we explain the numerical model we employed in Sec. II, then follows an explanation of the observables used to quantify our findings in Sec. III. In Sec. IV we then show and discuss our findings, in particular the lane formation in general, the funneling effect of the small particles, and an analysis of the formed lanes, as well as the onset of lane formation and parameter sets that facilitate it. Here we convert the numerically yielded values to the experimental setup. Last, we close with a conclusion in Sec. V.

II. MODEL

In this work we performed simulations without hydrodynamic interactions for quasi-two-dimensional systems (i.e.,

*Current address: Physics Department, University of Mainz, 55122 Mainz, Germany.

†peter.nielaba@uni-konstanz.de

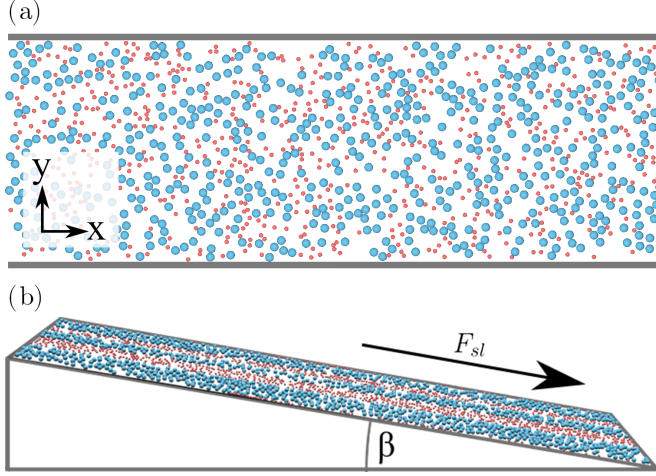


FIG. 1. (a) Top view of the random starting configuration. (b) Illustration of the setup. A channel with particles of two different diameters is placed on a slope with the angle β . The downhill slope force then acts as the driving force for the system. The small particles are shown in red and the large particles in blue.

three-dimensional systems in which movement is restricted to the plane). For this, we employed the Brownian dynamics algorithm to solve the overdamped Langevin equation.

According to Ref. [26], the positions of the particles are updated with

$$\mathbf{r}_i(t + \delta t) = \mathbf{r}_i(t) + \frac{D\delta t}{k_B T} \mathbf{F}[\mathbf{r}_j(t)] + \sqrt{2D\delta t} \mathbf{R}(t),$$

with δt the length of the time step, $k_B T$ the unit of the thermal energy, D the microscopic diffusion constant of a sphere, and $\mathbf{F}[\mathbf{r}_j(t)]$ the forces acting on particle i , consisting of the interaction with all particles j and the driving force. $\mathbf{R}(t)$ consists of standard normally distributed random numbers in the x and y directions. They satisfy the conditions $\langle R_k(t) \rangle = 0$ and $\langle R_k(t) R_l(t) \rangle = \delta_{kl}$, with $k, l \in \{x, y\}$.

The particles interact via the Weeks-Chandler-Andersen potential

$$V(r_{i,j}) = \begin{cases} 4\epsilon \left[\left(\frac{d_{\text{eff}}}{r_{i,j}} \right)^{12} - \left(\frac{d_{\text{eff}}}{r_{i,j}} \right)^6 \right] + \epsilon, & r \leq \sqrt[6]{2} d_{\text{eff}} \\ 0, & r > \sqrt[6]{2} d_{\text{eff}}, \end{cases}$$

where ϵ is the interaction strength (which we set to unity for simplicity), $r_{i,j}$ the center-to-center distance, and $d_{\text{eff}} = \frac{d_i + d_j}{2}$ the effective diameter between two particles i and j , with d_i and d_j the diameters of said particles. The centers of masses of both particle types are confined to a quasi-two-dimensional linear channel with hard walls in the y direction and periodic boundaries in the x direction. To simulate hard, reflecting walls, we employ the method described in Ref. [27], where particle positions which would overlap with the walls are redrawn according to the solution of the Smoluchowski equation in the half space. Before each simulation, all particles are placed randomly inside the channel [see Fig. 1(a)]. We set up our system as a channel on a slope, filled with small and large particles. An illustration of this setup is shown in Fig. 1(b), where the small particles are shown in red and the large ones in blue. To improve readability, we use red and blue for the

small and large particles, respectively, consistently throughout this work. From the start of a simulation, a driving force acts on the particles in the x direction. This force is the force of gravity

$$F_{sl} = F_{\text{small}} d_{sl}^3, \quad (1)$$

where $sl \in \{\text{small, large}\}$ and the force acting on the small particles F_{small} can be varied freely. With the particle diameters $d_{\text{small}} = \sigma$ and $d_{\text{large}} = a\sigma$, the difference in driving force scales as

$$\Delta F = F_{\text{large}} - F_{\text{small}} = (a^3 - 1)F_{\text{small}}. \quad (2)$$

The following five parameters were varied: the channel length L in the x direction and width W in the y direction, the driving force F_{small} (which corresponds to the slope angle), the area fraction $\phi = A_{\text{particles}}/A_{\text{channel}}$, and the diameter ratio a . For every simulation, we used the same amount of particles for both types.

In these simulations the length σ , energy $k_B T$, and diffusion constant D_0 of a sphere of diameter σ are used as reduced units. In the following, all quantities will be given in multiples of these units, as well as derived units, such as the diffusion time $\tau_D = \sigma^2/D_0$, which describes the average time in which a particle of diameter σ diffuses over a distance σ .

III. OBSERVABLES

In order to quantitatively analyze the order of the systems, we utilize the following quantities. The order parameter Φ_{lane} describes the degree of lane order in the drive direction, and we then count the lanes with a lane identification algorithm. We introduce the plug formation order parameter Φ_{plug} , which is a measure of the nonuniformity of the local particle density. Additionally, a neighboring cluster algorithm is used to analyze the most populated cluster sizes.

A. Lane formation parameter Φ_{lane}

The lane formation parameter is modeled after Ref. [9]. For a given time step and a particle i , a tube of width $w_t = \rho^{-\frac{1}{2}}$ is constructed. This width represents the average particle distance in the disordered system, where ρ is the total particle density, and the tube stretches across the whole length of the channel. An illustration of this tube is shown in Fig. 2. For every particle j within this tube, it is then checked whether it is of the same or the opposite particle type. If particle j is of the same particle type, a counter $n_{i,+}$ is incremented by unity, and if j is of the opposite particle type, $n_{i,-}$ is incremented. With these counters, the order parameter of the i th particle can be calculated by

$$\varphi_{\text{lane},i} = \left| \frac{n_{i,+} - n_{i,-}}{n_{i,+} + n_{i,-}} \right|.$$

This process is then repeated for every particle i , and the results can be averaged to obtain the lane formation parameter

$$\Phi_{\text{lane}} = \frac{1}{N} \sum_{i=1}^N \varphi_{\text{lane},i},$$

where N is the total particle number. For a randomly distributed configuration Φ_{lane} yields the value zero, while in a

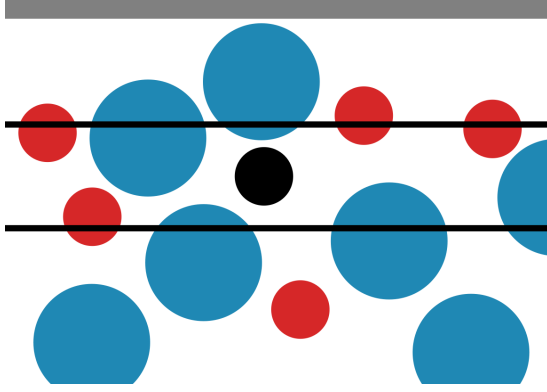


FIG. 2. Illustration of the tube that is used for the calculation of $\phi_{\text{lane},i}$. The small particles are shown in red and the large ones in blue. Particle i is marked in black and belongs to the small particles. The channel wall is shown in gray, and the tube of width w_i is marked in black.

system of perfect lanes it approaches unity. Since the lane formation order parameter increases in a sigmoid shape [compare Fig. 4(c) and Sec. S1 from the Supplemental Material [28]] for every parameter set presented in our work, we used the following fit to approach our data:

$$\Phi_{\text{lane}}(F) = \frac{p_1}{2} \left[\tanh \left(\frac{F - p_2}{p_3} \right) + 1 \right] + p_4, \quad (3)$$

where p_1 up to p_4 are fit parameters. This fit is chosen similarly to the one in Ref. [13]. We consider a system to have

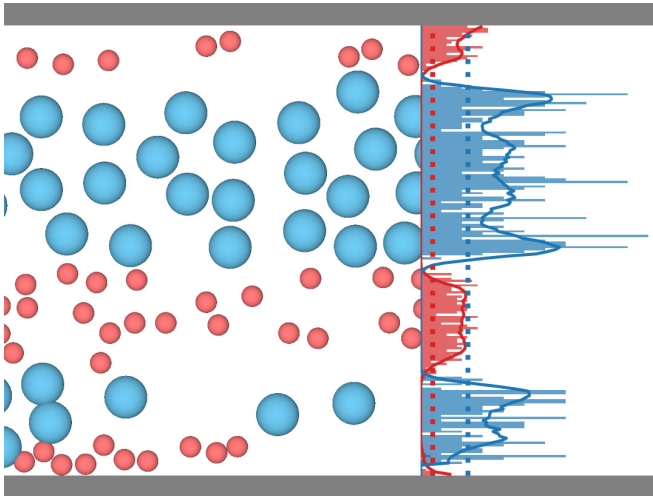


FIG. 3. Scheme of the lane identification. In the left part, a small section of a channel is shown with the small and large particles in red and blue, respectively. To the right, a histogram over the channel width of the local area density is shown. This area density is calculated for the whole channel length. The histogram is calculated only for the time step shown, while the solid line represents the average over the last quarter of this simulation (250 snapshots). This average is used for the actual lane identification calculation. The dotted lines represent the area density thresholds $\phi_{\text{eq},sl}$. The colors are matched with the left part of the figure, and the channel walls are shown in gray.

reached critical lane order when this order parameter reaches a value of $\Phi_{\text{lane,cr}} = 0.5$. The corresponding force necessary to reach this state is denoted as the critical force $F_{\text{small,cr}}$ and is read off the fit at this point. An uncertainty of the critical force can be obtained via the standard rules of error propagation [29].

B. Lane identification

To count the amount and analyze the widths of the lanes for a given time step, we calculated the particle density in the y direction. For this, the channel gets divided into bins of size $w_{\text{bin,lane}} = 0.1$. In each of these bins n the local particle area density gets calculated separately for both particle types:

$$\phi_{sl,n} = \frac{A_{\text{parts},sl,n}}{A_{\text{bin}}} = \frac{n_{sl,n} \pi \frac{d_{sl}^2}{4}}{w_{\text{bin,lane}} L}, \quad (4)$$

with $A_{\text{parts},sl,n}$ the area occupied by the particles of type sl in bin n , A_{bin} the area of a bin, and $n_{sl,n}$ the number of particles of type sl in bin n . Bin n will then be assigned to the particle type with the larger area density. For $n_{sl,\text{lane}}$ bins of the same type that are adjacent to one another, the lane width can be calculated as $n_{sl,\text{lane}} w_{\text{bin,lane}}$. The area densities calculated in Eq. (4) are averaged over the last quarter of the simulation. Additionally, a threshold area density of $\phi_{\text{eq},sl} = N_{sl,\text{tot}} \pi d_{sl}^2 / (4LW)$ (with $N_{sl,\text{tot}}$ the total amount of particles of type sl) is introduced. If the larger area density of a certain bin does not exceed the threshold density of its particle type $\phi_{\text{eq},sl}$, it will not be counted towards the lane widths or amounts. Figure 3 shows this calculation schematically.

C. Plug formation parameter Φ_{plug}

The plug formation parameter was introduced as a measure of the nonuniformity of the particle density in the channel. Hereby, the channel is divided both in the x and y directions into n_{bin} square bins. For ease of calculation, the side length of the bins l_{bin} is chosen so that L and W are integer multiples thereof:

$$L = n_{\text{bin},x} l_{\text{bin}}, \quad n_{\text{bin},x} \in \mathbb{N},$$

$$W = n_{\text{bin},y} l_{\text{bin}}, \quad n_{\text{bin},y} \in \mathbb{N},$$

$$n_{\text{bin}} = n_{\text{bin},x} n_{\text{bin},y}.$$

This parameter is similar to the band formation parameter in Ref. [13], but the radial bins are replaced with square ones. In contrast to Eq. (4), in each of these bins we calculate the combined area fraction of both the small and large particles

$$\phi_n = \frac{\pi \left(n_{\text{small},n} \frac{1}{4} + n_{\text{large},n} \frac{a^2}{4} \right)}{l_{\text{bin}}^2},$$

with $n_{\text{small},n}$ and $n_{\text{large},n}$ the number of large and small particles in bin n , respectively.

With all area fractions computed, the mean area fraction can then be calculated as

$$M = \sum_{i=n}^{n_{\text{bin}}} \frac{\phi_n}{n_{\text{bin}}},$$

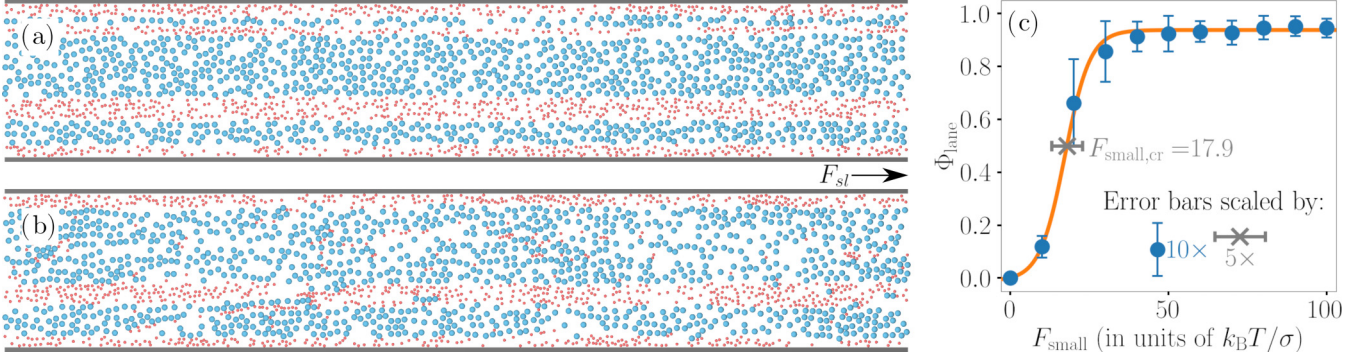


FIG. 4. Lane formation in a linear channel with width $W = 50$, area fraction $\phi = 0.30$ and diameter ratio $a = 2.0$. While at a larger driving force of (a) $F_{\text{small}} = 60$ the channel can be found in a very ordered state, a lower driving force of (b) $F_{\text{small}} = 20$ does not yet exhibit complete order. Panel (c) shows the course of the lane order parameter Φ_{lane} over the driving force F_{small} . The blue circles represent the data points that are averaged over 20 simulations each. The error bars for these data are multiplied by a factor of 10 for readability. The orange line is the fit to these data presented in Eq. (3), and the gray cross is the critical force obtained by this fit. The error bar for the critical force is magnified by a factor of 5.

with which we computed the variance as

$$S^2 = \sum_{i=n}^{n_{\text{bin}}} \frac{(M - \phi_n)^2}{n_{\text{bin}}}.$$

Last, the plug formation parameter is calculated as the ratio between the variance and the mean squared:

$$\Phi_{\text{plug}} = \frac{S^2}{M^2}.$$

A vanishing order parameter corresponds to a state where the particles are equally distributed between the bins and a value of unity to a state where half the bins are empty and the other half is equally occupied by the particles. A value of n_{bin} can be reached only when all particles are in a singular bin.

D. Cluster algorithm

We employed a neighboring cluster algorithm to determine the size of clusters inside the channels. For this, we computed the pairwise distances $r_{i,j}$ between particles of one particle type sl . A cluster was then defined to consist of particles with distances smaller than a cutoff distance $r_{i,j} < r_{\text{clus},sl}$. As the cutoff we chose the average particle distance for a single particle type in the ordered system. For this, we first compute the particle density per type $\rho_{sl} = N_{sl}/A_{\text{parts},sl}$, where N_{sl} is the total particle amount of type sl and $A_{\text{lanes},sl}$ the total area of the lanes of the same particle type. We calculated this area with the help of our results in Fig. 6 with $A_{\text{lanes},sl} = n_{\text{lanes},sl} w_{\text{lanes},sl}$ for a given channel width ($W = 50$ in Sec. IV D). Finally, the cutoff distance can be obtained via $r_{\text{clus},sl} = \rho^{-\frac{1}{2}}$. We define the cluster size as the amount of particles in a cluster. Afterward, we count the amount of particles that belong to a certain cluster size (where, e.g., two clusters of size 50 would amount to 100 particles). The most populated cluster size is then the one that contains the most particles. This algorithm was run for both particle types sl separately.

IV. RESULTS AND DISCUSSION

Starting from a random configuration, all of our simulations were run for $100\tau_D$. In Sec. S2 of the Supplemental Material [28], we conclude that these simulation times are sufficient for the order parameter Φ_{lane} to settle into a plateau. Most simulations were run with a time step of $\delta t = 5 \times 10^{-5}\tau_D$. Similarly to Ref. [30], if forces acting on the particles exceeded $F_{\text{max}} = d_{sl}D_{sl}k_B T/(10\delta t)$, the simulation had to be interrupted for reasons of numerical stability. This was mostly the case for systems that formed plugs. For these simulations, the length of the time step was reduced up to $\delta t = 1 \times 10^{-6}\tau_D$. The driving forces sampled to obtain the critical forces were in a range of $F_{\text{small}} \in [0, 100]$ in steps of $\Delta F_{\text{small}} = 10$. Additionally, if not stated otherwise, a number of 20 simulations was conducted for each parameter set. We found this amount to be sufficient after some testing, which will become apparent during the course of this work. These systems proved to show not much discrepancy in their steady states, as is evident by the small errors shown in, e.g., Fig. 4(c) (the error bars had to be scaled by a factor of 10 to improve readability).

A. Lane formation and critical force

By applying the driving force described in Eq. (1) onto the particles, we observed the formation of lanes. Figure 4(a) shows such a conformation. This particular simulation was performed with a channel width of $W = 50$, an area fraction of $\phi = 0.30$, and a diameter ratio of $a = 2.0$, and at a driving force of the small particles of $F_{\text{small}} = 60$. (This area fraction was chosen because we found the systems to be most prone to lane formation with this value, which we show in Sec. IV E 1.) In this case, the driving force of the large particles equates to $F_{\text{large}} = a^3 F_{\text{small}} = 480$. The small (red) and large (blue) particles separate into streams parallel to the drive direction. Hereby, the separated lanes move at different speeds, where the large particle lanes move at a velocity roughly fourfold that of the small particle lanes (compare Sec. S4 of the Supplemental Material [28]). Since the same amount of small and

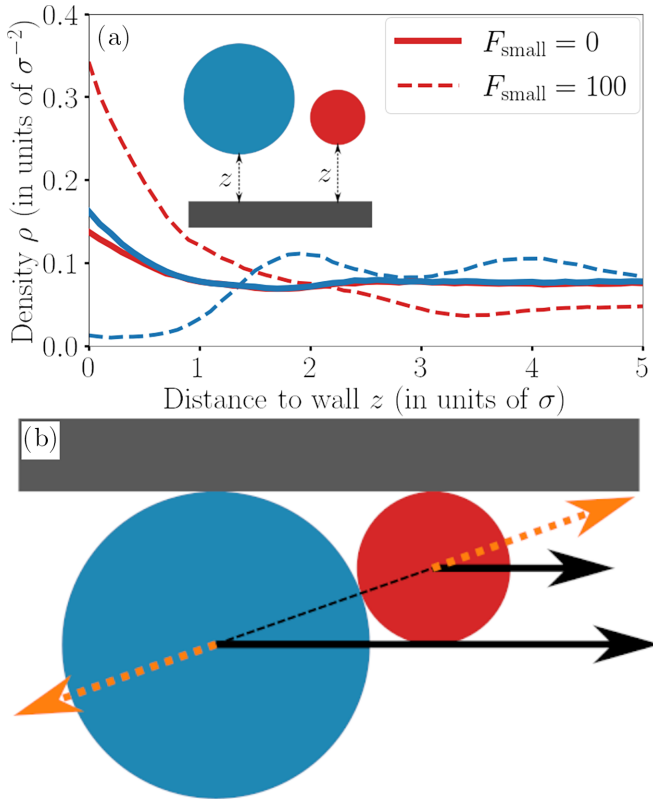


FIG. 5. (a) Particle density vs particle distance to the wall of the systems with $W = 50$. The red and blue curves represent the small and large particles, respectively. The solid lines show the equilibrium system ($F_{\text{small}} = 0$), and the dashed lines the system with a driving force of $F_{\text{small}} = 100$. These data were obtained by determining and averaging the particle densities at both the bottom and the top walls for all 20 different simulations. (b) The funneling effect in detail, where a large particle pushes a small particle to the wall, resulting in small particle boundary lanes. When a large particle (depicted in blue) overtakes a small particle (red), and both particles are close to the wall, the large particle will act as a funnel for the small particle. The gray bar at the top represents the wall, and the black arrows are the driving forces (not to scale). The dashed black line connects the centers of the two particles, and the orange arrows indicate the repulsive force that results from the particles moving closer than r_{cut} .

large particles was chosen for these simulations, we can see that the large particles occupy a larger area than the small particles. Additionally, the lanes at the walls consist only of small particles. In contrast, Fig. 4(b) shows a system at a force of $F_{\text{small}} = 20$, where order has not yet completely arisen. At the walls, we observe well-defined lanes consisting of the small particles, while we can also see lanes rather clearly in the bottom half of the channel. In the large particle lane in the top half, however, a few small particles are spread in the empty spaces' decreasing order.

Figure 4(c) depicts the order parameter Φ_{lane} in dependence on the driving force F_{small} . These values were obtained by averaging over the last quarter of all 20 simulations. When no driving force is applied, the systems stay in an unordered state with $\Phi_{\text{lane}} = 0$. After a small increase in the driving force, an immediate increase in order can be observed. At $F_{\text{small}} = 20$ the critical order parameter $\Phi_{\text{lane,crit}} = 0.5$ is

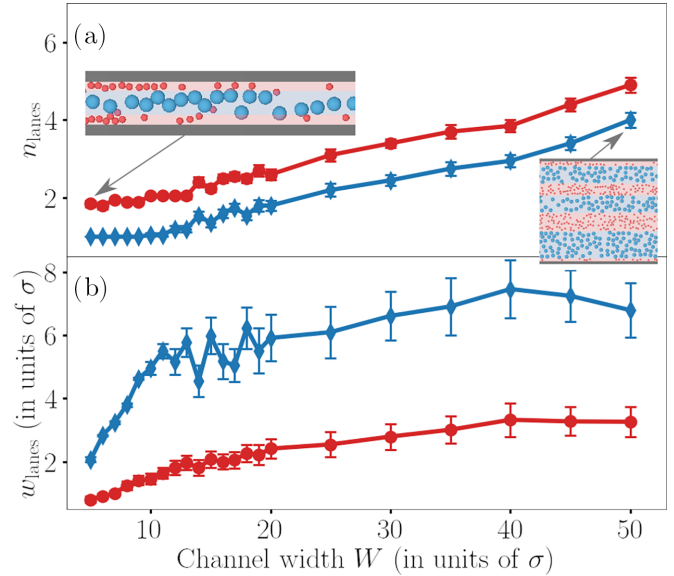


FIG. 6. (a) Amount and (b) width of lanes formed in the steady state in dependence on the channel width. The red circles and blue diamonds represent the small and large particles, respectively. With a widening of the channel, all amounts and widths increase, while for very thin channels only one configuration exists of two small particle boundary lanes and one large particle middle lane.

already surpassed [compare Fig. 4(b)], and at around $F_{\text{small}} = 40$ the parameter curve reaches a plateau. In the region of the largest increase in order parameter, we can see a larger error in the data points. This occurs since we are close to the critical force, where the most change in order occurs and systems are not settled into an ordered or unordered state. In the plateau region, the error decreases again. It should be noted that the error bars of the data points are scaled by a factor of 10 to improve readability. The actual error bars are remarkably small and would disappear inside the data points themselves (compare Sec. S1 of the Supplemental Material [28]). With the fit described in Eq. (3), which was already used in Ref. [13], we can approximate the course of the data points. We obtained the critical force for this system, which is where this fit surpasses a value of $\Phi_{\text{lane,crit}} = 0.5$, as $F_{\text{small,crit}} = 17.9$.

B. Funneling effect at the channel walls

In an equilibrium mixture of small and large particles, depletion forces describe a phenomenon where the large particles get pushed towards the walls of the system. This happens because the excluded volume for a small particle decreases when the large particles are closer to the walls, therefore increasing the entropy of the system [25]. In the ordered systems, however, it becomes apparent that the boundary lanes, i.e., the lanes at the channel walls, consist solely of the small particles. Figure 5(a) depicts the particle density for small (red) and large (blue) particles in dependence on the distance from the wall for the equilibrium (solid lines) as well as the nonequilibrium (dashed lines) state. The particle density was averaged over the last quarter of the simulation (250 time steps), all 20 simulations and also both the top and bottom wall. The distance z is the distance between the particle

surface and the wall. In the equilibrium state (solid lines), we find that very close to the wall the large particles exhibit a higher particle density compared to the smaller particles, which is likely due to the depletion forces in our system. This effect subsides very quickly towards the center of the channel, where the particle densities of both particle types become almost identical. In the nonequilibrium state (dashed lines) we observe this reverse drastically. Instead of a slight increase of the large particle density we see that the large particle density is very close to zero, while the small particle density is much higher than in the equilibrium state. This of course stems from the solely small particle boundary lanes.

We can explain this dramatic difference between equilibrium and nonequilibrium by closely looking at a large and a small particle that are both in proximity to the channel wall. Figure 5(b) depicts such a scenario schematically, and in Movie M1 of the Supplemental Material [28] we follow a small particle at the wall through the channel. When we look at the interaction between the two particles, the large particle acts like a funnel for the small particle. Since the centers of the particles are used to calculate the mutual repulsion, the resulting force vector of the small particle points partially into the wall while the force vector of the large particle points away from the wall. This interaction occurs only when the differently sized particles get pushed against each other from the driving force. Since high driving forces stabilize any lanes that form, these boundary lanes also survive in the longer time frame of a complete simulation ($100\tau_D$). All simulations at the highest driving force of $F_{\text{small}} = 100$ ended in a state where the boundary lanes were populated by small particles.

C. Lane widths and amounts

Figures 6(a) and 6(b) show the amount and width of the lanes formed at the highest driving force of $F_{\text{small}} = 100$. The values result from averaging over the last quarter of the 20 simulations with different starting configurations.

It is apparent that the amount of the lanes n_{lanes} increases with the channel width. The two curves for the small particles (red circles) and the large particles (blue diamonds) increase completely synchronously, as well as their respective errors. This is because the small particles always occupy the boundary lanes, which means there is always exactly one additional small particle lane ($n_{\text{lanes,small}} - n_{\text{lanes,large}} = 1$; see Sec. IV B). For very thin channels, the systems only exhibit one configuration, i.e., two lanes of small particles at the edges and one large particle lane in the middle. This results in the flat curve for low channel widths and a vanishing error. By widening the channels, however, we can see a steady increase in n_{lanes} .

In Fig. 6(b) one can see that the lane width w_{lanes} does not increase as continuously as the number of lanes. While for very thin channels the lane width of the large particles increases quite sharply, the curves flatten rather quickly for wider channels. Since for a given channel $W = \sum_{sl} w_{\text{lanes},sl} n_{\text{lanes},sl}$ has to hold (if one does not account for the area density threshold $\phi_{\text{eq},sl}$ from Sec. III B, which excludes some bins), this of course fits well with a steadily increasing number of lanes. If the width of the lanes stays constant over all channel widths, the number of lanes would necessarily have to increase. The large increase at low channel widths

can be explained with the opposite scenario: The number of lanes stays at a similar value for a few data points, which means that the width of those lanes has to increase. Since the large particles exhibit only one possible lane in the thinnest channels, that lane has to widen faster than the lanes of the small particles. Since our systems were designed with the same number of small and large particles $n_{\text{small}} = n_{\text{large}}$, the total area occupied by the large particles is fourfold the area of the small particles with a diameter ratio of $a = 2.0$. This results in the fact that the large particle lanes are wider than the small particle lanes, where the ratio between the two curves seems to level off at approximately two. After being very low at small channel widths, the error increases very rapidly and remains at a similarly large value for the course of the plots starting from $W \approx 15$. This means that there is no single stable width that a lane prefers to fall into. This is because at such high driving forces, once a lane is formed, it is very unlikely to merge with another lane of the same particle type.

D. Onset of lane formation

We conducted a set of 20 short simulations with a simulation length of $7.5\tau_D$, channel width $W = 50$ and area fraction $\phi = 0.30$. There we found that lanes form via a mechanism where small chains of particles develop, enlarging in drive direction by moving into the “slipstreams” of one another, where they form very thin lanes. These thin lanes then push each other aside, creating slanted lane boundaries of higher local particle density and leaving empty spaces behind. When this process is finished and the particles inside a lane are allowed to diffuse in the y direction, the stable lane state is reached with a more uniform particle density again. Figure 7(a) shows a state with emerging clusters. We can see that, at a first glance, the configuration looks rather well distributed, although locally there are a few small chains of the same particle type. A particle can move more freely in drive direction if it moves behind a particle of the same particle type. The lanes found in Ref. [18] look quite similar to these short chains. In contrast to our lanes, their lanes have reached the steady state, however. These smaller clusters then combine to form longer and slightly wider chains, which could be described as lanes that don’t span the whole channel length. They then further combine by pushing lanes of the opposite type aside, creating large boundaries that span across the channel at an angle. Such a configuration can be seen in Fig. 7(b). Finally, when the short and thin lanes are combined, the steady state with lanes spanning across the whole channel is reached [compare Fig. 4(a)]. Each particle in this state can move in the slipstream of another particle of the same particle type (which is supported by the periodic boundaries) and a stable state is reached. This whole process can also be observed in Movie M2 of the Supplemental Material [28].

To support our findings, we looked at the plug formation order parameter Φ_{plug} described in Sec. III C, the most populated cluster size from Sec. III D and also at the mean absolute fluctuations perpendicular to drive direction $\langle |v_y| \rangle$ over time. The fluctuations are calculated by dividing the particle displacement by the time step.

Figure 8(a) shows the cluster size populated by the most particles as a measure of cluster size over time. (Note that

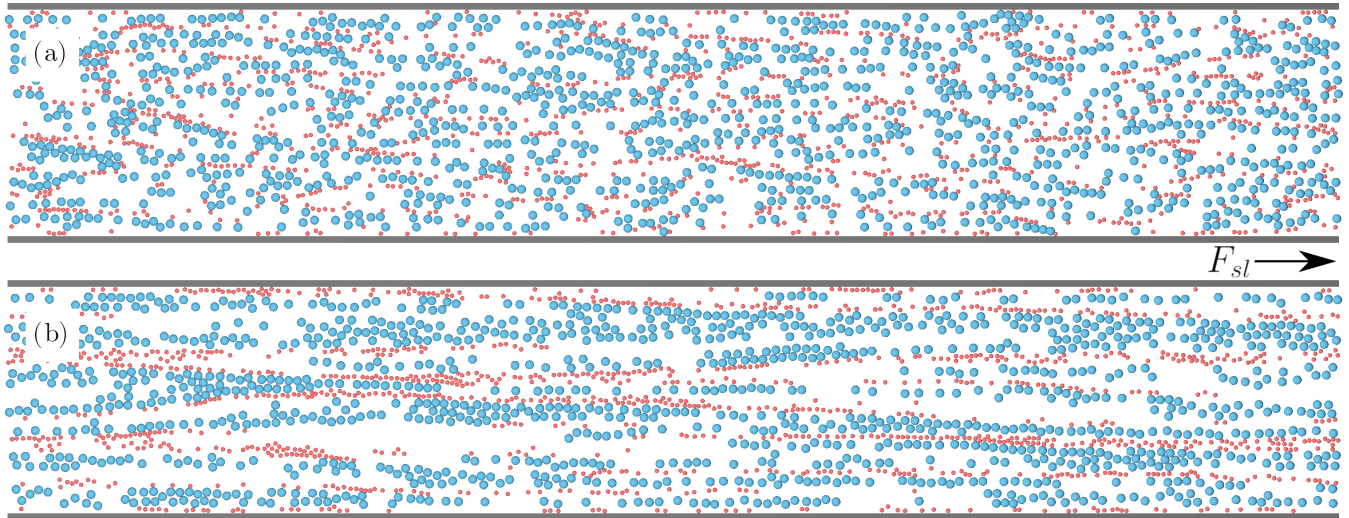


FIG. 7. Snapshots of the formation of lanes, taken at (a) $t = 0.1125\tau_D$ and (b) $t = 0.75\tau_D$. This calculation was performed with a channel width $W = 50$ and an area fraction $\phi = 0.30$.

noninteger values can be reached because the values are averaged over 20 simulations.) We can see that the red and blue data show very similar curves. From their shared starting point, the most probable cluster sizes increase quite quickly to their maximum values. This maximum value is marked with the dashed purple line across the three plots. The fact that the curve shows a maximum can be attributed to the slanted particle boundaries from Fig. 7(b) that push particles of the same particle type closely together. When these particles are allowed to diffuse in the lanes that form in the last step, the cluster size decreases to a stable value, signifying that the system reached the steady state. The fact that the two cluster size curves coincide this well can be attributed to the choice of the cluster cutoff presented in Sec. III D.

The parameter Φ_{plug} in Fig. 8(b) is a measure of the nonuniformity of the local particle density. The side length of the quadratic bins was chosen to be $l_{\text{bin}} = 5$. At the start of the simulation the particles are very homogeneously distributed, therefore, the value of Φ_{plug} remains low. After applying the driving forces, it, however, increases very rapidly, almost vertically. This vertical jump appears because in the very short time frame, and no collisions between the small and large particles occur. Therefore, the faster large particles get closer to the small particles without any particles pushing each other aside. The curve then keeps increasing at a slower pace until it reaches its peak at roughly $1\tau_D$. This peak symbolizes the point with the most apparent lane boundaries and is marked with the dotted vertical black line. After the particles are all pushed into their respective lanes, the parameter decreases again, which shows that a steady state is reached. In both Figs. 8(a) and 8(b) the maximum values represented by the dotted black and the dashed purple line occur at similar points in time. This indicates a strong correlation between the two, which can be attributed to the emergence of lane formation by slanted particle boundaries.

In the steady state, the particles are confined to their respective lanes. Therefore, not a lot of movement in the direction perpendicular to drive direction can be observed. In contrast to this, during the lane formation process, Fig. 8(c) shows a

great deal of vertical movement of both particle types. Since the particles need to get pushed from the disordered state into lanes, we see large values for the average absolute vertical fluctuations $\langle |v_y| \rangle$ at the start of the simulation. For both particle types, these values reach a stable state at roughly $1\tau_D$. The difference in values of the small and large particles can be attributed to the difference of the diffusion coefficients $D_{sl} = k_B T / (3\pi\eta d_{sl})$, which are dependent on the particle diameter d_{sl} .

The process of forming lanes happens rather quickly, at times of roughly $1\tau_D$. In systems with a lower driving force or different system parameters, e.g., with a longer channel or a higher particle density, we suspect this process to slow down. It remains to be examined exactly how much this process is affected by a change of parameters. However, we see this as additional indication that our chosen simulation times are sufficient.

E. Lane facilitating parameter sets

By changing the system parameters such as the channel width or length, or the particle density, the formation of lanes can be facilitated. Fortunately, the sigmoid course of the lane formation parameter Φ_{lane} is consistent through different parameter sets and systems (compare Sec. S1 of the Supplemental Material [28]). This means that we can easily compare the critical force $F_{\text{small,crit}}$ of these systems to evaluate their tendency to reach a state of lane order. Hereby, a lower critical force indicates that a system has a higher tendency to reach an ordered state. While we obtained an optimal value for the area fraction and the width of the channel, we found an increasing diameter ratio to always facilitate lane formation. A finite-size study of the channel length can be found in Sec. S3 of the Supplemental Material [28]. Here we show that for an area fraction of $\phi = 0.30$, an elongation of the channel above $L = 300$ would not change the tendency towards lane formation. The common parameters chosen for these simulations were a channel length and width of $L = 300$ and $W = 20$, an

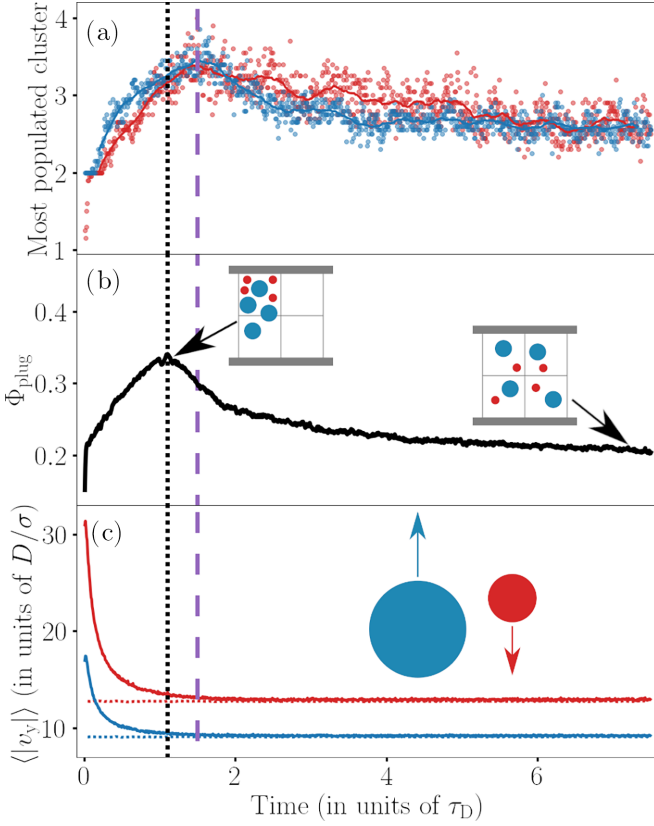


FIG. 8. Lane formation onset over time. (a) The cluster size occupied by the most particles over time. Red and blue data points show small and large particle clusters, respectively. The red and blue lines are running averages over the data points that act as guides to the eye. The dashed vertical purple line represents the maxima of the data. During the formation of lanes, clusters of particles form that get resolved to a certain degree in the stable state. (b) The plug formation parameter Φ_{plug} over time, represented by the black line. The vertical dotted black line represents the maximum of the average curve. Before lanes can form from clusters, particles move in vertical direction via slanted lane boundaries, which increases the plug formation parameter. (c) Average absolute vertical fluctuations $\langle |v_y| \rangle$ over time. The red and blue curve represent the data for small and large particles, respectively. During the lane formation process, the particles have to move greatly in the vertical direction. When lanes are formed, the particles can settle in at stable vertical fluctuations.

area fraction of $\phi = 0.30$, and a particle diameter of $a = 2.0$, if not stated otherwise.

1. Dependence on the area fraction and channel width

The area fraction of the channels is defined as

$$\phi = \frac{A_{\text{parts}}}{A_{\text{channel}}} = \frac{\frac{1}{4}\pi n_{\text{small}} + \pi n_{\text{large}}}{LW},$$

with A_{parts} the area of the particles, A_{channel} the area of the channel, and n_{small} and n_{large} the particle numbers of the small and large particles, respectively. Both particle types were kept to the same amount in all our simulations.

Figure 9(a) shows $F_{\text{small,crit}}$ in dependence on the area fraction. The tendency towards lane formation first increases in the range from $\phi = 0.10$ to 0.30, after which it decreases

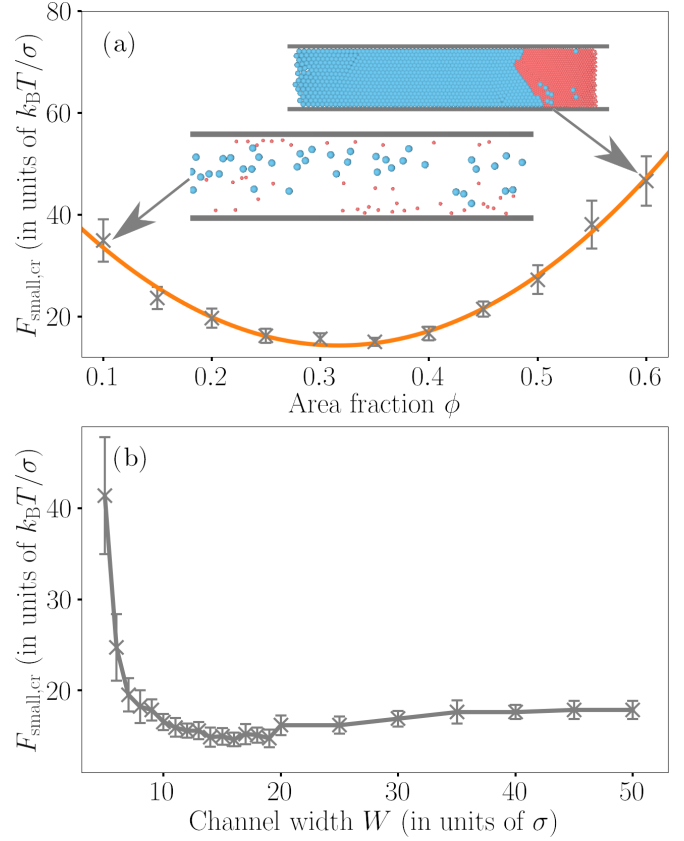


FIG. 9. (a) $F_{\text{small,crit}}$ over ϕ . The gray crosses represent the data points with their respective error bars and the orange line is a quadratic fit to these data. The larger errors at the edges arise from a subset of the simulations resulting in states with no lanes. (b) $F_{\text{small,crit}}$ over W . The gray crosses represent the data points with their respective error bars, and the gray line acts as a guide to the eye. The large value for the thinnest channels can be explained by the lack of particles to fill three complete lanes, while the slightly higher values of the plateau for the wide channels lead to the assumption of a lane-stabilizing effect of the channel walls.

again for channels with more particles. This leads to the conclusion that there is a sweet spot where lane formation is most favorable. The lowest value for the critical force was reached at an area fraction of $\phi = 0.35$ with $F_{\text{small,crit}} = 15.0$. The quadratic fit that was applied to approach the data points exhibits a minimum for $\phi \approx 0.32$ with a value of $F_{\text{small,crit}} = 14.3$. For this reason, an area fraction of $\phi = 0.30$ was chosen for most simulations. In the systems with a low area fraction, the channels consist of an insufficient amount of particles to form lanes that span across the whole channel. This means that it becomes much more likely for particles to move into the “slipstream” of a particle of a different type, which decreases Φ_{lane} . A cutout of a snapshot of such a system can be seen in the bottom inset in Fig. 9(a). The order of these systems is therefore not as consistently at the same value, which results in their larger error bars. On the other side of the plot, one can see much larger error bars for the systems of large area fractions. Since some of the simulations with this parameter set form plugged steady states (compare top inset in Fig. 9), their lane formation parameter decreases significantly, which

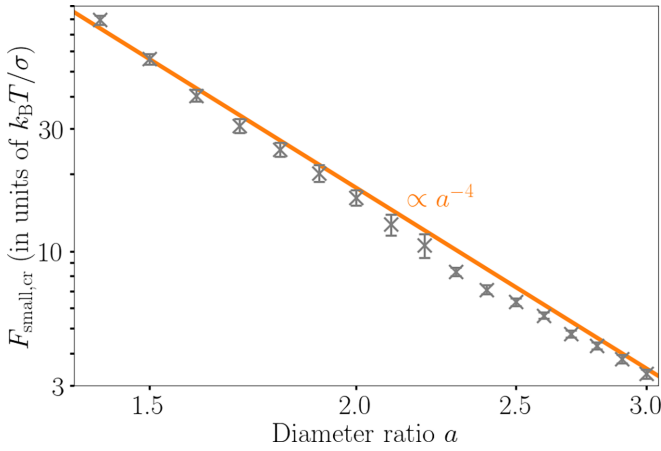


FIG. 10. Log-log plot of the $F_{\text{crit,small}}$ dependence on the particle diameter ratio a . The gray crosses represent the data points with their respective error bars, and the orange line is a power-law fit to these data.

in turn increases the critical force and its error. This curve progression of the critical force with a minimum is consistent with the reentrance effect found in Ref. [14]. It should be noted that the values we obtained for large area fractions should be taken with a grain of salt. In Sec. S3 of the Supplemental Material [28], we discuss that with an increase of the area fraction from $\phi = 0.30$ to 0.50 , an elongation of the channel does indeed lead to an increase of the critical force. This leads us to the assumption that the increase of the critical force beyond $\phi = 0.30$ would be steeper for higher channel lengths.

The dependence on the channel width is shown in Fig. 9(b). Very thin channels exhibit a very large critical force. This can be explained because the channels are so thin that there are barely enough particles to form three lanes [compare top left inset in Fig. 6(a)]. A minimum of the critical force curve can be found at $W \approx 15$. The critical force for wider channels increases and seems to hit a plateau for the limit of infinitely wide channels. This implies the existence of lane-stabilizing effects introduced by the hard walls, which also fits the snapshot in Fig. 4 where the lanes closer to the walls show higher lane order.

2. Dependence on the particle diameter

By changing the diameter ratio a , we can influence the driving force difference ΔF without changing F_{small} . Equation (2) shows that for an increasing diameter ratio, we can expect the tendency towards lane formation to increase. Figure 10 shows the dependence of the critical force $F_{\text{crit,small}}$ on a in a log-log plot. As expected, the tendency towards lane formation increases with a growing diameter ratio. We found a power-law fit of

$$F_{\text{crit,small}}(a) = p_5 a^{-4} \quad (5)$$

to describe the data fairly well.

The Péclet number Pe is a quantity describing the ratio between particle transport and diffusion. With the mean velocity $\langle v \rangle \approx \langle v \rangle_D = D_{sl} F / (k_B T)$, where $\langle v \rangle_D$ is the mean drift

velocity of a free particle, we find for the Péclet number

$$Pe_{sl} = \frac{d_{sl} \langle v \rangle}{D_{sl}} = \frac{d_{sl} F}{k_B T},$$

with the chosen reduced units $k_B T$ and $d_{\text{small}} = \sigma$ equaling unity. (We discuss in Sec. S4 in the Supplemental Material [28] that for very large forces, the assumption of particles moving with the mean free drift velocity $\langle v \rangle \approx \langle v \rangle_D$ of a free particle holds. For forces around the critical point, however, we can expect discrepancies of up to 30%.) We can then write for the difference in Péclet number of the two particle species

$$\begin{aligned} \Delta Pe &= d_{\text{large}} F_{\text{large}} - d_{\text{small}} F_{\text{small}} \\ &= F_{\text{small}} (a^4 - 1). \end{aligned} \quad (6)$$

We can see that in Eq. (5), as well as in Eq. (6), the critical force $F_{\text{crit,small}}$ has an a^{-4} dependence. This shows us that the critical point is closely related to the Péclet number difference.

3. Exemplary value calculation for the experimental setup

For an experimental implementation, we want to demonstrate an exemplary calculation that translates the values from reduced units to SI units. For this calculation, we again neglect hydrodynamic interactions and all friction between the particles and the walls or the floor. We conduct this calculation for the system parameters that proved to be most prone to lane formation, i.e., the parameter set with the lowest critical force. These values are the channel width of $W = 15$ and the area fraction of $\phi = 0.30$. Since an increase of the diameter ratio would always ease lane formation (within reasonable limits), we settle for a value of $a = 2.0$. For this parameter set, we yielded the critical force $F_{\text{small,cr}} \approx 15$. We additionally need to assume some experimental system values. These values were selected in accordance to Ref. [31]. For the temperature, we chose room temperature $T = 293$ K, the mass density of silica $\rho_{\text{m,SiO}_2} = 2.65$ g/cm³, and the water as solvent $\rho_{\text{m,H}_2\text{O}} = 1.00$ g/cm³, and the size of the small particles as $d_{\text{small,exp}} = 4$ μm .

With this, we can calculate the force in SI units corresponding to the numerically yielded $F_{\text{small,cr}}$:

$$F_{\text{exp}} = F_{\text{small,cr}} \frac{k_B T}{d_{\text{small,exp}}} = 1.52 \times 10^{-14} \text{ N}.$$

Since we need to account for buoyancy, the downward force acting on a small particle equates to $F_z = \pi/6 \times d_{\text{small,exp}}^3 (\rho_{\text{m,SiO}_2} - \rho_{\text{m,H}_2\text{O}}) g = 5.42 \times 10^{-13}$ N with g the gravitational constant. With the equation for the downhill-slope force $F_{\text{ds}} = F_z \sin(\beta)$ and β the angle of the slope [see Fig. 1(b)], we can calculate the angle that needs to be set for the experimental setup to achieve the driving force F_{exp} :

$$\begin{aligned} F_{\text{ds}} &= F_z \sin(\beta) \stackrel{!}{=} F_{\text{exp}}, \\ \beta &= \arcsin \left(\frac{F_{\text{exp}}}{F_z} \right), \\ \beta &= 1.02^\circ. \end{aligned}$$

This calculation is highly sensitive to the particle diameter $d_{\text{small,exp}}$, since it appears in the arcsin function as a

factor of $d_{\text{small,exp}}^{-4}$. With small particles with half the diameter $d_{\text{small,exp}} = 2 \mu\text{m}$, the angle increases to 26.6° .

V. CONCLUSION

In this work we investigated the lane formation of simulated colloids that are driven by gravity. A difference in driving force between the two particle types was achieved by a difference in their diameters.

We observed a phenomenon at the hard walls of the channel, which we call the funneling effect. When two particles move in proximity to a wall, the difference in their diameters leads to a difference in distance of their respective centers to the wall. Because of this, the small particle can wedge between the large particle and the wall, pushing the large particle out towards the center of the channel. As a result, we found the edges of the channels to always be occupied by small particles. This is a stark contrast to equilibrium systems where entropic depletion forces push the large particles to the walls rather than the small ones [25].

Quantitative analysis of the lane amount and width shows that with an increase of the channel width, more and wider lanes form. The difference between small and large particle lanes was also found to be constant at unity as a direct result of the funneling effect. We found the lanes to be stable during our simulation time of $100\tau_D$ once they formed. However, it would be very interesting to see if lanes might switch or merge in the infinite time limit.

The onset of lane formation was shown to consist of several steps. At first, particles of the same type form short chains in drive direction. These shorter chains then combine to lengthen and widen. At a certain point, those longer clusters cannot pass through clusters of the opposite particle type anymore because of their considerable length and width. In this next step, the particles need to form slanted boundaries between the elongated clusters, in which the particles can move perpendicularly to drive direction to combine with other clusters into lanes of the same particle type.

Additionally, we scanned the parameter space consisting of area fraction, channel width, and particle diameter for a parameter set ideal for lane formation. For the area fraction, we found that the critical force follows a quadratic curve,

with a minimum at $\phi \approx 0.30$. At very high area fractions, a subset of the simulations showed a plugged state, increasing the critical force. An ideal channel width could be reached at $W \approx 15$, where the stabilizing effect of the channel walls reaches its maximum. At very low channel widths, it becomes harder for the particles to form lanes because of their low amount and the very thin and perfect lanes that need to form. With an increase in channel width past the minimum, lanes form less easily, and in the wide channel limit the curve of the critical forces seems to reach a plateau. Since with our force model the diameter ratio a directly influences the driving force difference ΔF , we cannot directly examine the influence of the diameter ratio on lane formation. With our model in mind, however, we could show that the critical force curve follows a simple $p_5 a^{-4}$ dependence, i.e., with an increase of the diameter ratio lanes form more easily. This makes it closely related to the difference in Péclet number, which follows the relation $\Delta Pe = F_{\text{small}}(a^4 - 1)$.

We expect that this model of force difference could be implemented in experiments with a mix of differently sized particles on a slope. The angle at which the channel is tilted would directly influence the driving force. We were able to calculate a rough estimate of the angle needed for the slope with the parameter set we found most well suited for lane formation. Since hydrodynamic interactions, which we neglected in our work, counteract the formation of lanes (compare Ref. [24]), we suspect our estimates to be too low. We, however, expect that the parameter study we conducted will facilitate the search for lanes in experiments. Additionally, an experimental setup with a seesaw motion could be envisaged, which could lead to much longer observation times. The computational counterpart could prove an intriguing subject for a follow-up work with our model.

ACKNOWLEDGMENTS

This research was funded by the Deutsche Forschungsgemeinschaft DFG (Projects No. NI259/16-1, No. ER341/13-1, and No. LE315/27-1). The authors gratefully acknowledge the Gauss Centre for Supercomputing e.V. for funding this project by providing computing time through the John von Neumann Institute for Computing (NIC) on the GCS Supercomputer JUWELS [32] at Jülich Supercomputing Centre (JSC).

-
- [1] C. Feliciani and K. Nishinari, *Phys. Rev. E* **94**, 032304 (2016).
 - [2] L. Lian, X. Mai, W. Song, Y. K. K. Richard, Y. Rui, and S. Jin, *Fire Safety J.* **91**, 918 (2017).
 - [3] S. Yajima, K. Yoshii, and Y. Sumino, *J. Phys. Soc. Jpn.* **89**, 074003 (2020).
 - [4] I. D. Couzin and N. R. Franks, *Proc. R. Soc. London B* **270**, 139 (2003).
 - [5] F. L. Memarian, J. D. Lopes, F. J. Schwarzendahl, M. G. Athani, N. Sarpangala, A. Gopinathan, D. A. Beller, K. Dasbiswas, and L. S. Hirst, *Proc. Natl. Acad. Sci. USA* **118**, e2117107118 (2021).
 - [6] R. Jose and L. Santen, *Phys. Rev. Lett.* **124**, 198103 (2020).
 - [7] T. Shimaya and K. A. Takeuchi, *Phys. Rev. E* **99**, 042403 (2019).
 - [8] K. Klymko, P. L. Geissler, and S. Whitlam, *Phys. Rev. E* **94**, 022608 (2016).
 - [9] B. Heinze, U. Siems, and P. Nielaba, *Phys. Rev. E* **92**, 012323 (2015).
 - [10] D. Jin and L. Zhang, *Acc. Chem. Res.* **55**, 98 (2022).
 - [11] P. Stengele, A. Lüders, and P. Nielaba, *Phys. Rev. E* **106**, 014603 (2022).
 - [12] M. Wagner, S. Roca-Bonet, and M. Ripoll, *Eur. Phys. J. E* **44**, 43 (2021).
 - [13] T. Vater, M. Isele, U. Siems, and P. Nielaba, *Phys. Rev. E* **106**, 024606 (2022).

- [14] J. Chakrabarti, J. Dzubiella, and H. Löwen, *Phys. Rev. E* **70**, 012401 (2004).
- [15] J. Dzubiella, G. P. Hoffmann, and H. Löwen, *Phys. Rev. E* **65**, 021402 (2002).
- [16] H. Frusawa, *Entropy* **24**, 500 (2022).
- [17] M. Rex and H. Löwen, *Phys. Rev. E* **75**, 051402 (2007).
- [18] T. Vissers, A. Wysocki, M. Rex, H. Löwen, C. P. Royall, A. Imhof, and A. van Blaaderen, *Soft Matter* **7**, 2352 (2011).
- [19] F. Kogler and S. H. L. Klapp, *Europhys. Lett.* **110**, 10004 (2015).
- [20] K. R. Sütterlin, A. Wysocki, A. V. Ivlev, C. R ath, H. M. Thomas, M. Rubin-Zuzic, W. J. Goedheer, V. E. Fortov, A. M. Lipaev, V. I. Molotkov *et al.*, *Phys. Rev. Lett.* **102**, 085003 (2009).
- [21] U. Sarma, S. Baruah, and R. Ganesh, *Phys. Plasmas* **27**, 012106 (2020).
- [22] C. W. W achtler, F. Kogler, and S. H. L. Klapp, *Phys. Rev. E* **94**, 052603 (2016).
- [23] A. Wysocki and H. Löwen, *J. Phys.: Condens. Matter* **23**, 284117 (2011).
- [24] M. Rex and H. Löwen, *Eur. Phys. J. E* **26**, 143 (2008).
- [25] D. Rudhardt, C. Bechinger, and P. Leiderer, *Phys. Rev. Lett.* **81**, 1330 (1998).
- [26] D. L. Ermak and Y. Yeh, *Chem. Phys. Lett.* **24**, 243 (1974).
- [27] H. Behringer and R. Eichhorn, *Phys. Rev. E* **83**, 065701(R) (2011).
- [28] See Supplemental Material at <http://link.aps.org/supplemental/10.1103/PhysRevE.108.034607> for lane formation order parameter curves for different parameter sets; whether we can say that our systems are in the steady state; whether finite size effects occur; and what the mean drift velocity of our colloids is.
- [29] J. Tellinghuisen, *J. Phys. Chem. A* **105**, 3917 (2001).
- [30] Y.-G. Tao, W. K. den Otter, J. T. Padding, J. K. G. Dhont, and W. J. Briels, *J. Chem. Phys.* **122**, 244903 (2005).
- [31] Y. Alsaadawi, A. Eichler-Volf, M. Heigl, P. Zahn, M. Albrecht, and A. Erbe, *Eur. Phys. J. E* **44**, 23 (2021).
- [32] D. Alvarez, *JLSRF* **7**, A183 (2021).